Characterization of the Ferroelectric Phase of Encapsulated $Hf_{1-x}Zr_xO_2$ Using a Combination of Synchrotron-based X-ray Techniques and Polarization Measurements

Vineetha Mukundan[1], Steven Consiglio[2], Kandabara Tapily[2], Dina Triyoso[2], Gert Leusink[2], Arthur Woll[3], Karsten Beckmann[1], Nathaniel Cady[1], and Alain C. Diebold[1]

[1] SUNY Polytechnic Institute, Colleges of Nanoscale Sciences & Engineering, Albany, NY 12203, USA

[2] TEL Technology Center, America, LLC., Albany, NY 12203, USA

[3] Cornell High Energy Synchrotron Source (CHESS), Ithaca, NY 14853, USA

MOTIVATION

Ferroelectricity in hafnia-based dielectrics was recently discovered by Böscke et al. and has been attributed to the stabilization of a polar orthorhombic phase [1]. Characterization of this ferroelectric phase of ultra-thin films of hafnia-based dielectrics, in both metal-insulator-metal (MIM) and metal-insulator-semiconductor (MIS) film stacks, is a critical part of advancing their application in both ferroelectric random-access memory (FeRAM) and ferroelectric field-effect transistor (FeFET) devices [2]. Applications in steep slope transistors based on negative capacitance effect (NC-FET) [3] and analog synapses for deep neural network training [4] are also under investigation. Doping with various elements or alloying with similar oxides such as zirconia can enable ultra-thin hafnia-based films to be stabilized in different structural phases, which have direct bearing on ferroelectric properties for these different applications. Alloying hafnia with zirconia enables high remnant polarization values for a wide range of composition ratios not seen with other dopants [5].

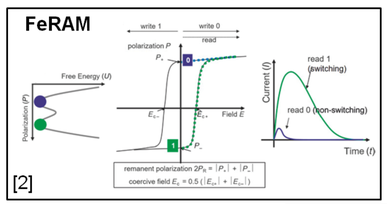

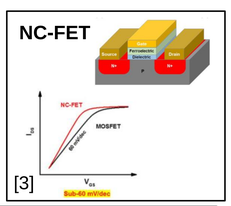

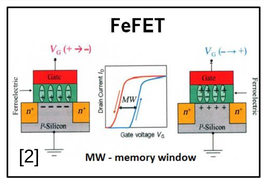

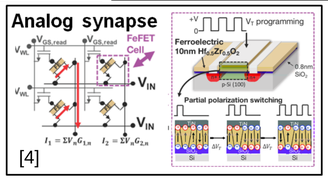

METROLOGY

These FE materials have a strong structural correlation and this entails the use of different metrological techniques to study them.

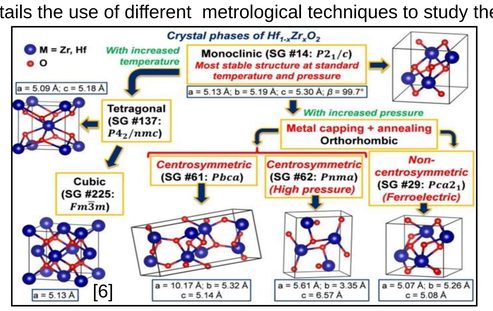

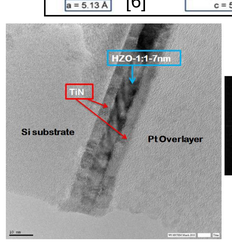

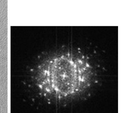

Electron Microscopy:

TEM cross-section of the HZO 1:1 film is shown here.

The FFT shows a mixture of different phases which is also confirmed by our GI-XRD data and EXAFS data.

X-ray Diffraction: Grazing Incidence geometry

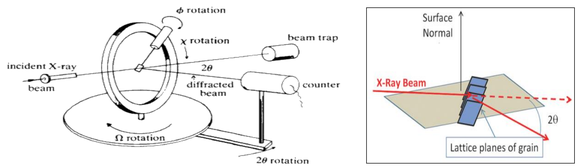

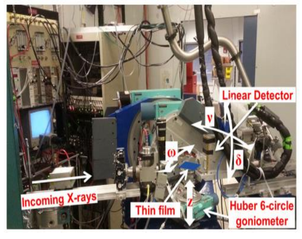

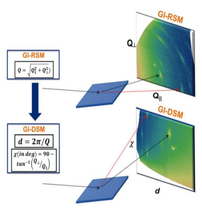

G2 beamline at CHESS, Cornell

The x-ray beam energy was in the range of 10.8KeV to 11.3keV and had the dimension of 2mm (horizontal) by 0.2mm (vertically). Samples are staged at the center of the 6-circle diffractometer using a vacuum chuck. A series of Ω-2v scans were acquired at different values of tilt of the detectors. The use of a linear detector for the GI-XRD enables coverage of wide range of the reciprocal space at one scan point while acquiring high quality data. Using Matlab and Python codes, motor spec data was converted to reciprocal space maps and distance space maps [6, 7].

X-ray fine structure spectroscopy (EXAFS): Grazing incidence geometry

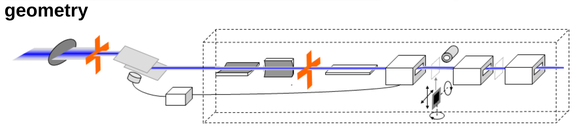

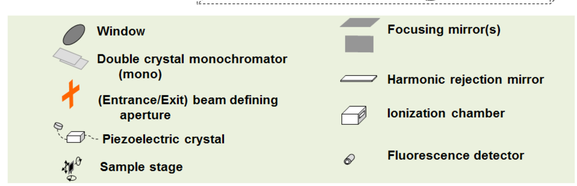

Spectra were recorded to probe the local chemistry at the Hf L3 edge and Zr K edge at 6-BM, NSLS-II, BNL. Scans were performed at room temperature. Demeter package which includes several programs such as Athena, Artemis, Atoms and FEFF was used for plotting and data analysis [8].

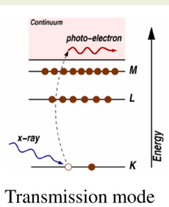

Transmission mode

Polarization Measurements:

A semiconductor analyzer with a waveform generator and fast measurement unit was deployed to apply pulses in the microsecond regime and measure the corresponding current response. The polarization was extracted from the current response in the positive-up negative-down (PUND) measurement scheme.

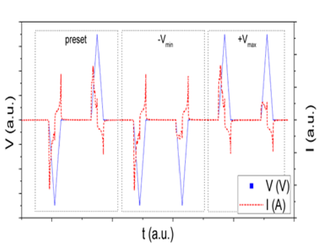

RESULTS

- EXAFS on 7nm thick $Hf_{1-x}Zr_xO_2$ samples were recorded for a set varying in composition (Hf:Zr) and thickness with 1:1 composition.
- In the composition plot, the second shell corresponding to Hf-Hf scattering paths shows significant changes. As the ZrO_2 content is increased, the local disorder increases [9-11] while undergoing structural reconstructions.

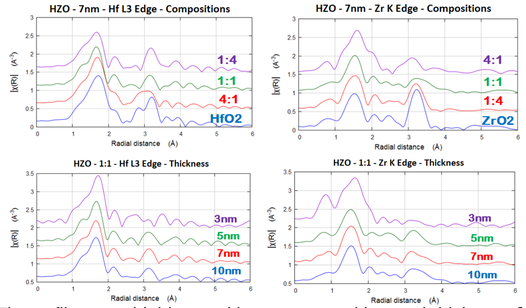

- These films are highly sensitive to composition and thickness [12]. The tables summarize the structures for different compositions and thicknesses. For 50% zirconia and below, there is a suppression of the M phase in MIM compared to MIS. For 7nm and 10nm MIM stack, there is suppression of the M phase.

M= Monoclinic ($P2_1/c$), T = Tetragonal ($P4_2/nmc$), O= Orthorhombic ($Pca2_1$)

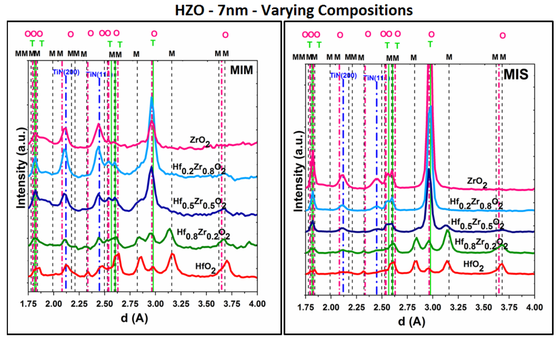

Composition	MIS	MIM
ZrO_2	T	T
$Hf_{0.2}Zr_{0.8}O_2$	T	T
$Hf_{0.5}Zr_{0.5}O_2$	M+T+O	T+O
$Hf_{0.8}Zr_{0.2}O_2$	M+O	M+O
HfO_2	M+O	M+O

Thickness	MIS	MIM
3nm	Too thin	Too thin
5nm	T+O	T+O
7nm	M+T+O	T+O
10nm	M+T+O	M+T+O

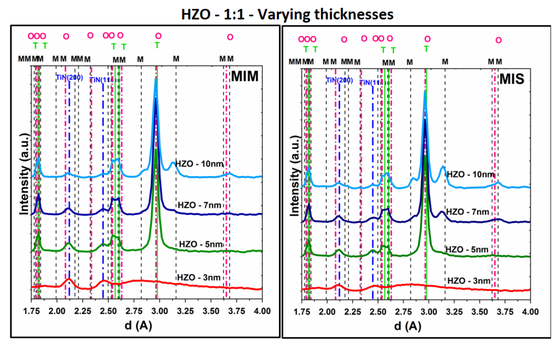

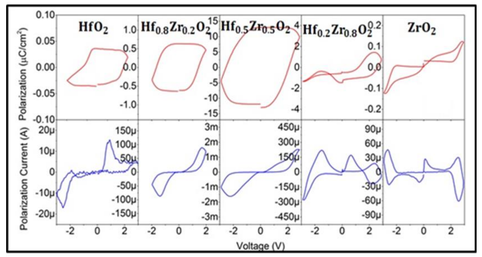

- Polarization measurements in MIS stacks were reported by Dey et al [8] and confirmed the ferroelectric behavior in composition 1:4 although the XRD data indicated the formation of the tetragonal phase.
- Polarization measurements show changes in ferroelectric behavior in HZO samples as MIM stacks with changes in composition ratio of 1:4, 1:1 and 4:1 and in both hafnia and zirconia films [13,14].

SUMMARY

- $Hf_{1-x}Zr_xO_2$ nanoscale films were investigated for their structural correlation to ferroelectric behavior which is attributed to the formation of the non-centrosymmetric orthorhombic phase.
- For logic and memory application of ferroelectric $Hf_{1-x}Zr_xO_2$, effect of composition, thickness, types of bottom electrode (MIM vs. MIM) on structural and electrical properties were investigated.
- Synchrotron based x-ray metrology techniques such as GI-I-XRD and EXAFS are essential for elucidating both the long range and short range atomic ordering in these ultra-thin films.
- Detailed analysis are underway to understand the correlation between the percentage content of the different phases in these $Hf_{1-x}Zr_xO_2$ dielectric thin films with their ferroelectric or anti-ferroelectric behavior.

REFERENCES

1. T. S. Böscke et. al., Applied Physics Letters, 99(10), 102903 (2011).
2. T. Mikolajick et. al., MRS Bulletin, 43(5), 340-346, (2018).
3. M. A. Alam et. al., Appl. Phys. Lett. 114, 090401 (2019)
4. M. Jerry et al., In 2017 IEEE International Electron Devices Meeting (IEDM) (pp. 6-2). IEEE, (2017, December).
5. L. Xu et. al., Journal of Applied Physics, 122(12), 124104, (2017).
6. S. Dey et al., International Conference on Frontiers of Characterization and Metrology for Nanoelectronics, 223-225, (2017).
7. S. Dey et. al., Journal of Applied Physics, 120(12), p.125304, (2016).
8. B. Ravel et. al., Journal of synchrotron radiation, 12(4), 537-541, (2005).
9. S. B. Erenburg et. al., Journal of Experimental and Theoretical Physics, 126(6), pp.816-824, (2018).
10. D. Y. Cho et. al., Physical Review B, 82(9), p.094104, (2010).
11. M. A. Sahiner et. al., Thin Solid Films, 515(16), pp.6548-6551, (2007).
12. M. H. Park et. al., Adv. Mater., 27: 1811-1831, (2015).
13. R. D. Clark et. al., In Meeting Abstracts (No. 16, pp. 696-696). The Electrochemical Society, (July 2018).
14. V. Mukundan et. al., MRS Advances, pp.1-7 (2019).

ACKNOWLEDGEMENTS

V.M. acknowledges the TEL Technology Center America, LLC for funding support. The authors also acknowledge the contribution of Dr. Tom Murray from CNSE, Dr. Jean-Jordan Sweet from BNL and Dr. Bruce Ravel from NIST. This work is based on research done at CHESS supported by NSF and NIH/NIGMS under the NSF award DMR-1332208 and used 6-BM, of the NSLS II, a U.S. DOE Office of Science User Facility operated for the DOE Office of Science by BNL under Contract No. DE-SC0012704.